RSC Advances

PAPER

View Article Online
View Journal | View Issue

Cite this: *RSC Adv.*, 2023, **13**, 22054

Synthesis of Sb_2S_3 nanosphere layer by chemical bath deposition for the photocatalytic degradation of methylene blue dye

Mohammed M. Gomaa, *[a] Mohamed H. Sayed, [ab] Mahmoud S. Abdel-Wahed [c] and Mostafa Boshta [a]

An antimony tri-sulfide Sb_2S_3 nanosphere photocatalyst was effectively deposited utilizing sodium thiosulfate and antimony chloride as the starting precursors in a chemical bath deposition process. This approach is appropriate for the large-area depositions of Sb_2S_3 at low deposition temperatures without the sulfurization process since it is based on the hydrolytic decomposition of starting compounds in aqueous solution. X-ray diffraction patterns and Raman spectroscopy analysis revealed the formation of amorphous Sb_2S_3 layers. The scanning electron microscopy images revealed that the deposited Sb_2S_3 has integrated small nanospheres into sub-microspheres with a significant surface area, resulting in increased photocatalytic activity. The optical direct bandgap of the Sb_2S_3 layer was estimated to be about 2.53 eV, making amorphous Sb_2S_3 appropriate for the photodegradation of organic pollutants in the presence of solar light. The possibility of using the prepared Sb_2S_3 layer in the photodegradation of methylene blue aqueous solutions was investigated. The degradation of methylene blue dye was performed to evaluate the photocatalytic property of Sb_2S_3 under visible light. The amorphous Sb_2S_3 exhibited photocatalytic activity for the decolorization of methylene blue solution under visible light. The mechanism for the photocatalytic degradation of methylene blue has been proposed. Our results suggest that the amorphous Sb_2S_3 nanospheres are valuable material for addressing environmental remediation issues.

Received 29th March 2023
Accepted 5th July 2023

DOI: 10.1039/d3ra02062b

rsc.li/rsc-advances

Introduction

Nanostructured metal sulfides (NMSs) have recently attracted considerable interest in a number of applications owing to their distinct optoelectronic and catalytic properties.[1–3] These properties depend greatly on the morphologies and dimensions of the prepared materials,[4] making these materials feasibly useful in various applications, such as dye removal from wastewater,[5] energy conversion and storage,[6] rechargeable lithium-ion batteries,[7] hydrogen evolution,[8,9] and photocatalysts.[10] Metal sulfide nanostructures with controllable nanoshapes, such as particles, wires, sheets, flakes,[11] hollow spheres,[12] and core–shell structures,[13] have been regarded as potential cost-effective, chemically stable, and nontoxic semiconducting materials for catalytic applications.[8,14,15]

Spherical structures are a type of functional material that has a high surface area and small charge transport lengths.[16] Spherical structures are classified as basic or complex based on their structural complexity. Simple spherical formations are one thing, as are solid spheres and single-shelled hollow spheres.[17] Because of their customizable physical and chemical properties, spherical structures offer significant structural advantages for electrochemical applications. High complexity hollow spherical micro/nanostructures have drawn significant interest in both theoretical studies and practical applications. Nanostructured spherical materials showed enhanced electrochemical performance and structural stability compared to the other alternative structures.[16,18] The variety of the material forms offers more potential for increasing functionality than simple spherical structures, which enhances the photocatalytic performance of the active material.[15,16]

Metal sulfide materials have received a great deal of attention and study.[19–25] Among metal sulfides, antimony sulfides with different phases have received significant attention owing to their unique physical properties, low toxicity, abundance, and environment-friendliness, making them ideal candidates for solar cells and environmental applications.[26] Sb_2S_3 can have either an amorphous phase known as metastibnite or a crystalline phase known as stibnite, depending on the synthesis process. The amorphous Sb_2S_3 phase has a direct energy gap (E_g) in the range of 1.7–2.8 eV, while the E_g for the crystalline

[a]*Solid State Physics Department, National Research Centre, Dokki, Giza 12622, Egypt. E-mail: dr.metwalyg@gmail.com; Tel: +201272110812*

[b]*Molecular and Fluorescence Spectroscopy Lab, Central Laboratories Network, National Research Centre, Dokki, Giza 12622, Egypt*

[c]*Water Pollution Research Department, National Research Centre, Dokki, Giza 12622, Egypt*

phase ranges between 1.7 and 1.8 eV.[27] In terms of application, the photocatalytic performance of antimony compounds in the degradation of organic pollutants is still less efficient compared to other photocatalysts based on noble metals and phosphides.[3,28] In this regard, limited work has been devoted to using Sb_2S_3 as a photocatalytic material in the degradation of organic dyes.[29] In addition, amorphous and crystalline Sb_2S_3 in the powder form have displayed an enhanced photocatalytic degradation of organic dyes with visible light.[30,31] To the best of our knowledge, nanosphere Sb_2S_3 layers have not been investigated before in the photocatalytic degradation of organic dyes. The innovative characteristic quality within the Sb_2S_3 layers that causes the separation of those materials will secure their multiple usages and consequently reduce the overall treatment cost. Therefore, the creation of a more sufficient synthesis process for the inorganic nanosphere is important. Additionally, amorphous Sb_2S_3 layers are still quite uncommon and require more investigation.[32] Most of the chemical methods are suitable for preparing antimony sulfides in powder form with different phases.[9,33] Among these approaches, chemical bath deposition (CBD) is one of the most attractive deposition processes because it is simple, cost-effective, and suitable for depositing a large area of thin films. The demand for an approach to prepare thin films with a high specific area and controlled morphology is still a major challenge, and it will open doors to diverse prospects for environmental application.

Methylene blue is a persistent organic pollutant material that is used in textile manufacturing for dyeing objectives in the modern world. Waste from textile manufacturing deteriorates water resources, and is detrimental to humans and other living organisms because of the potential for eye diseases, kidney diseases, and skin diseases. These types of pollutants cannot be removed by conventional treatment.[34] Thus, the development of novel methods is needed to address this concern. One of the main issues in the photocatalyst process is the separation and recovery constraint of the photocatalyst from the effluent after the treatment process. Therefore, this work overcomes this issue through the deposition of Sb_2S_3 on a glass substrate as thin layers.

A feasible CBD approach was used in this study to effectively produce Sb_2S_3 nanosphere layers directly without the need for a sulfurization process. The structural, morphological, optical, and catalytic properties of the resulting Sb_2S_3 layers were investigated. The unique nanosphere shape of the Sb_2S_3 layers acts as a powerful photocatalyst for the photodegradation of methylene blue dye.

Experimental

Sb_2S_3 layer deposition

Initially, the chemical bath deposition (CBD) technique was employed to prepare a nanosphere-structured antimony sulfide layer. The used glass substrates were cleaned in an ultrasonic bath with acetone, ethyl alcohol, and distilled water separately for 20 minutes, followed by nitrogen gas drying. As the starting solution, antimony chloride ($SbCl_3$ – Sigma Aldrich) was dissolved in acetone and dropped into 1 M sodium thiosulfate ($Na_2S_2O_3 \cdot 5H_2O$ – Sigma Aldrich) aqueous solution with continuous stirring, producing clear and homogeneous solution. During the synthesis process, the cleaned substrates were vertically dipped in the solution bath at a low deposition temperature and pH of 6. After 10 minutes, the colorless solution was transformed into an orange–yellow solution with the Sb_2S_3 layer formed on the substrate surface due to the adsorption and nucleation of antimony sulfide on the substrate. To remove the residual precipitation, the deposited layers were washed several times with distilled water. Fig. 1 shows a schematic representation of the chemical bath deposition process of the nanosphere-structured Sb_2S_3 layer.

The deposition was performed in a relatively weak acidic solution at pH approximately 3. Hence, the mechanism of the nanosphere-structured as-deposited Sb_2S_3 layer using thiosulphate solution is based on the hydrolytic decomposition of antimony(III) thiosulphate complexes of $Sb_2(S_2O_3)_3$ formed in aqueous media as a result of the reaction between $SbCl_3$ and $Na_2S_2O_3$, as in the following reactions:[35,36]

$$2SbCl_3 + 3Na_2S_2O_3 \rightarrow Sb_2(S_2O_3)_3 + 6NaCl \quad (1)$$

$$2Sb^{3+} + 3S_2O_3^{2-} \rightarrow Sb_2(S_2O_3)_3 \quad (2)$$

Thiosulphate ions in acidic media can gradually release S^{2-} ions during hydrolytic decomposition, according to the reactions.

$$S_2O_3^{2-} + H^+ \rightarrow S + HSO_3^- \quad (3)$$

$$S + 2e^- \rightarrow S^{2-} \quad (4)$$

The released excess S^{2-} ions react with the Sb^{3+} ions released from the thiosulphate complexes upon hydrolysis, reacting on the glass substrates to form orange-yellow Sb_2S_3:

$$2Sb^{3+} + 3S^{2-} \rightarrow Sb_2S_3\downarrow \quad (5)$$

Characterization of the as-deposited Sb_2S_3 layer

In this study, Cu Kα radiation at 40 kV and 40 mA was used to conduct X-ray diffraction (XRD) investigations for the structural

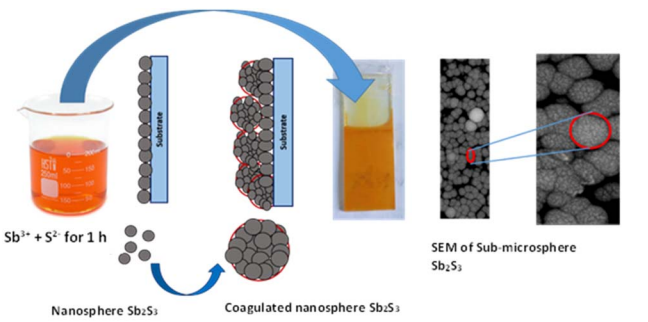

Fig. 1 Schematic description of the synthesis of nanosphere Sb_2S_3 layers.

and phase examination of the Sb_2S_3 layer. The morphology of the deposited layers was imaged using FEI Quanta 250 FEG scanning electron microscopy (SEM). X-Ray photoelectron spectroscopy (XPS) data were collected using a K-ALPHA (Themo Fisher Scientific, USA) spectrometer to determine the chemical composition and electronic states of the Sb_2S_3 layer. The Raman study was carried out using a Witec Alpha 300 RA confocal Raman microscope with laser excitation at 532 nm. Optical measurements were performed using a UV/VIS/NIR spectrophotometer (Jasco V770).

Evaluation of the photocatalytic performance of the Sb_2S_3 layers

The photocatalytic activity of the as-prepared Sb_2S_3 this film was recognized by methylene blue photodegradation as a model of the refractory organic contaminants. For this goal, the Sb_2S_3 sample was fixed on a 2 cm-height edge inside a 150 mL beaker by a silicon adhesive. After that, the beaker was filled with 90 mL of 10 mg L^{-1} methylene blue solution, and stirred by a magnetic stirrer. Then, the beaker was irradiated vertically using a UVA-CUBE 400 sunlight simulator (Dr Hönle AG UV Technology, Germany). At definite time intervals, online measurement of methylene blue removal was performed by spectrophotometer (Jasco 630). The creation of the redox reactive species by the Sb_2S_3 thin film slide excited by solar irradiation was studied by 1 mmol ammonium oxalate (AO), *para*-benzoquinone (*p*-BQ) and isopropyl alcohol (IPA) as the hole (h^+) scavenger agent, the superoxide radical ($O_2^{\bullet -}$) scavenger and as the hydroxyl radical $^{\bullet}OH$ scavenger, respectively.

Results and discussion

Structural and elemental composition properties

The XRD and Raman data of the produced Sb_2S_3 layer are presented in Fig. 2. It is seen that no obvious characteristic peaks were observed in the XRD spectrum of the as-deposited Sb_2S_3 layer by the CBD method, indicating that the deposited layer has an amorphous phase structure, as shown in Fig. 2(a).

The obtained results are in agreement with the previously reported XRD data for the Sb_2S_3 deposited by CBD in different media and different starting sulfur precursors,[37,38] and the reported amorphous Sb_2S_3 phase prepared by thermal evaporation technique.[39] Fig. 2(b) shows the Raman spectrum of Sb_2S_3 before and after photocatalytic test. The appearance of a broad peak in the range of 250–350 cm^{-1} and centered at the position 289 cm^{-1} indicated the existence of Sb_2S_3 in the amorphous phase, as described in prior studies.[40–42] The Raman spectra clearly indicate that no structural changes are observed in the Sb_2S_3 layers after the test.

This work used X-ray photoelectron spectroscopy (XPS) measurements to investigate the elemental compositions and electronic states of a nanosphere Sb_2S_3 layer. Fig. 3(a) presents the high-resolution XPS spectrum of Sb 3d for the deposited Sb_2S_3 layer, which has two main peaks located at 529.93 eV and 539.22 eV. These two peaks were assigned to the spin–orbit splitting of Sb $3d_{5/2}$ and Sb $3d_{3/2}$, respectively, which was separated by 9.29 eV. The binding energies values and the separation by spin orbit coupling suggest that Sb bound to S remains in the Sb^{3+} oxidation state, which coincides well with the reported values of Sb^{3+} in the Sb_2S_3 lattice. These values are within the range of the binding energy values reported by various research groups for the Sb^{3+} state in the Sb_2S_3 material.[42–44]

In addition, the high-resolution spectrum of the S core level presents two peaks, a main peak located at 162.11 eV and a shoulder peak positioned at 160.98 eV, which correspond to the $2p_{1/2}$ and $2p_{3/2}$ of S^{2-}, respectively, and separated by 1.13 eV as shown in Fig. 3(b). These values imply the existence of unsaturated sulfur atoms on the Sb–S and S–S bonds in Sb_2S_3.[45,46] XPS analysis confirmed that the deposited sample is the Sb_2S_3 material. The results of the XRD, Raman and elemental composition and chemical states analysis confirmed that the deposited samples are an amorphous Sb_2S_3, which is in agreement with the reported studies.[47,48]

Morphological characterization

The SEM images with different magnifications of the deposited samples on the glass are displayed in Fig. 4. The morphological properties of the deposited Sb_2S_3 indicate a preference for the eventual integration of small nanospheres into sub-microspheres. It is clear that the nanospheres are randomly distributed and have different sizes. The irregularly stacked and merged small nanospheres resulted in consolidated sub-microspheres ranging in size from 0.25 μm to 0.5 μm. Moreover, as can be seen in the magnified images, the sub-microspheres have a rough surface and have a propensity to develop pores within the spheroidal units (Fig. 4(d)). These sub-

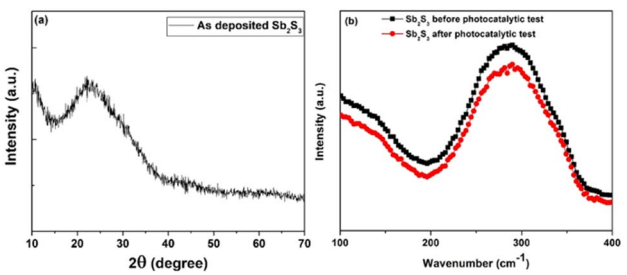

Fig. 2 (a) XRD pattern of Sb_2S_3 and (b) Raman spectra of Sb_2S_3 before and after the photocatalytic test.

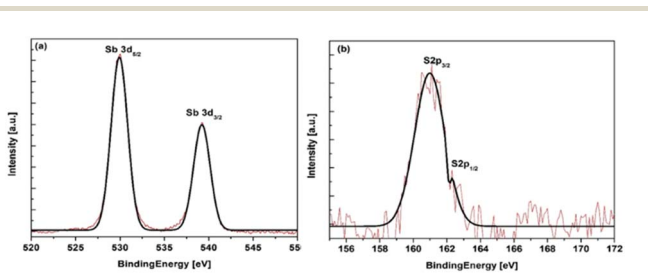

Fig. 3 XPS spectra of the core levels for deposited Sb_2S_3: (a) Sb 3d and (b) S^2.

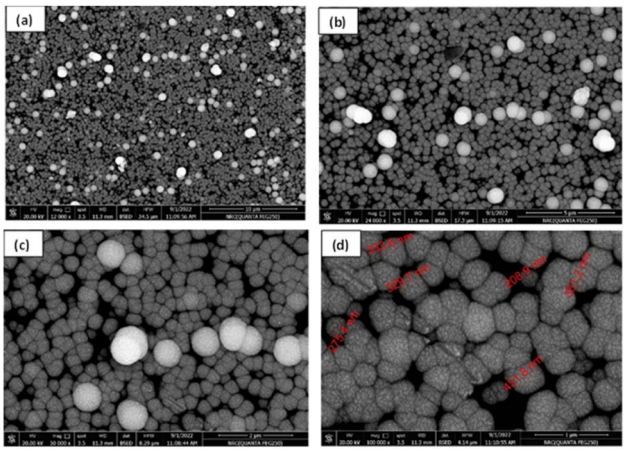

Fig. 4 (a)–(d) SEM images with different magnifications of the Sb_2S_3 layer.

microspheres are anticipated to offer more practical anchoring sites and allow for the adsorption of organic dyes, which could enhance the photocatalytic activity.[12,49,50]

Optical properties

Fig. 5(a) displays the optical transmittance and reflectance spectra of the chemically deposited Sb_2S_3 layer as a function of wavelength ranging between 250 to 2500 nm. The following formula is utilized to calculate the absorption coefficient (α).

$$\alpha = \frac{1}{t}\ln\left[\frac{(1-R)^2}{2T} + \sqrt{\frac{(1-R)^4}{4T^2} + R^2}\right] \quad (6)$$

where T, R, and t are the transmission, reflectance, and film thickness, respectively. The Tauc equation has been presented as a mathematical equation to demonstrate the relationship between the optical energy gap and the energy of the incident photon.

$$\alpha h\nu = A(h\nu - E_g)^n \quad (7)$$

where α is the absorption coefficient, $h\nu$ is the photon energy, A is a constant, E_g is the band gap, and n is an index that has values of 1/2, 2, 3/2, and 3, depending on the electronic transition of the deposited material.[51] The plot of $(\alpha h\nu)^2$ *vs.* $h\nu$ for the directly allowed transition is used to calculate the band gap (E_g) of the Sb_2S_3 layers by extrapolating the linear portion near the onset of the absorption edge to the energy axis, as shown in Fig. 5b. The estimated value of E_g for the Sb_2S_3 layer was 2.53 eV, which agrees with the reported values.[27,52] A similar range of the E_g value would qualify the benefit of this material in the solar photocatalytic applications.[42]

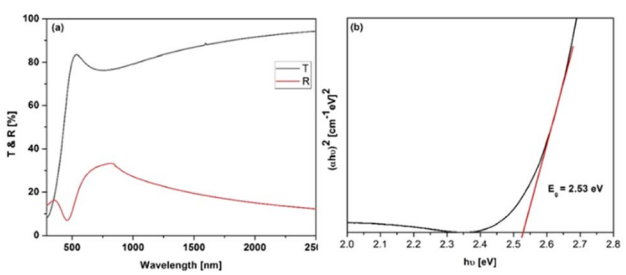

Fig. 5 $(\alpha h\nu)^2$ *versus* photon energy ($h\nu$) for the nanosphere Sb_2S_3 layer.

Catalytic properties

The photocatalytic activity of the prepared Sb_2S_3 thin film was performed with 10 mg L^{-1} methylene blue as the module organic compound at a pH of 6.5, and 5 cm^2 area of the Sb_2S_3 thin film. The change in relative concentration (C/C_o) of methylene blue with time is presented in Fig. 6. In the presence of the prepared Sb_2S_3 thin film and solar light irradiation, the methylene blue (C/C_o) decreased with time. The prepared Sb_2S_3 thin film was activated by the absorbed solar light, which initiated the photoproduction of e^-/h^+ that was employed in the photodegradation of methylene blue. In contrast, the presence of only solar light irradiation without the prepared Sb_2S_3 thin film resulted in the insignificant photolysis of methylene blue.

The produced redox species that was generated after exciting the prepared Sb_2S_3 layer by solar light was identified by appending 1 mmol of the individual scavenger agents (IPA, AO and *p*-BQ) with 10 mg L^{-1} methylene blue and the Sb_2S_3 sample. Fig. 7 represents the effect of the scavengers on methylene blue removal in the presence of scavengers and without scavengers. The hydroxyl radical ($^{\bullet}OH$) is a primary active species, the superoxide radicals ($O_2^{\bullet -}$) is a secondary active species, and the hole (h^+) is a third active species. Therefore, the suggested mechanism of the photocatalytic reactions is specified by the subsequent equations:

$$Sb_2S_3 \xrightarrow{h\nu} Sb_2S_3(h^+,\ e^-) \quad (8)$$

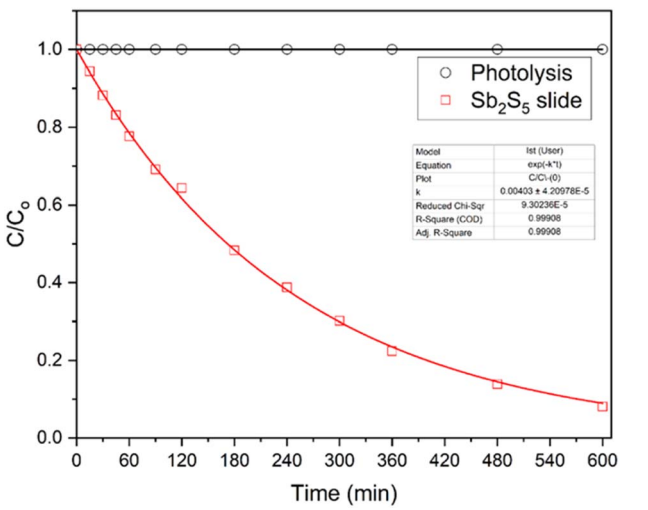

Fig. 6 Photocatalytic activity of the prepared Sb_2S_3 sample, methylene blue = 10 mg L^{-1}, pH 6.5 and Sb_2S_3 sample (5 cm^2).

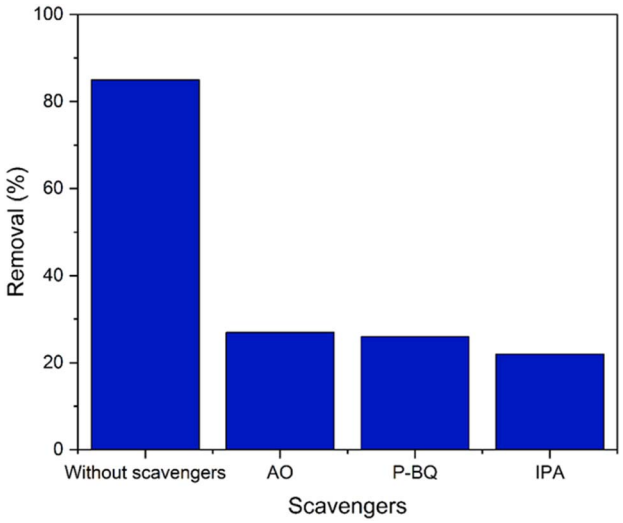

Fig. 7 Effect of scavengers on the methylene blue removal efficiency.

$$^{-}OH + h^{+} \rightarrow {}^{\cdot}OH \quad (9)$$

$$O_2 + e^{-} \rightarrow O_2^{\cdot -} \quad (10)$$

$$\text{Methylene blue} + h^{+} + {}^{\cdot}OH + O_2^{\cdot -} \rightarrow \text{indermediate} \rightarrow \text{degraded products} \quad (11)$$

One of the most important factors that influence the practical application of the photocatalysts is the reusability test, which will lead to a cost-effective treatment process. So, the photocatalytic activity of the prepared Sb_2S_3 layer (5 cm^2), pH natural and 10 mg L^{-1} methylene blue on reuse experiments is offered in Fig. 8. An insignificant decrease in the methylene blue photodegradation removal was observed with up to five runs. This demonstrates that the prepared Sb_2S_3 layer can maintain its photocatalytic activity and stability for more times in treatment processes, as confirmed by Raman measurements.

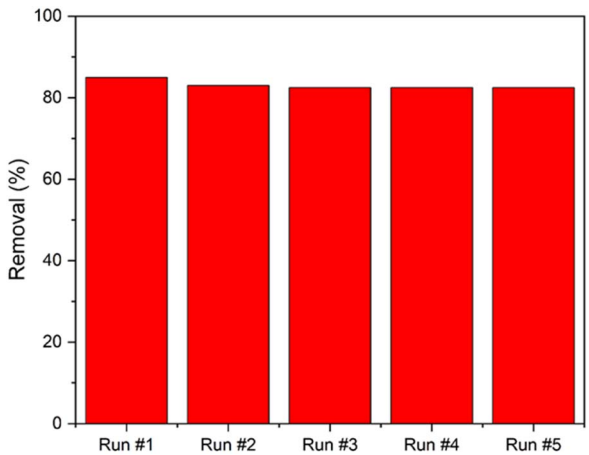

Fig. 8 Photocatalytic activity of the Sb_2S_3 sample (5 cm^2), natural pH and 10 mg L^{-1} methylene blue on reuse experiments.

Conclusions

In summary, the antimony tri-sulfide Sb_2S_3 nanosphere layer was synthesized directly by chemical bath deposition method at low deposition temperature and large scale for efficient photocatalytic application. The deposited layer was characterized by various characterization techniques that demonstrated that Sb_2S_3 has an amorphous phase structure with good morphological and optical properties. X-ray diffraction and Raman analysis showed the amorphous structure of the Sb_2S_3 films. Optical analyses revealed that the Sb_2S_3 layer has an optical energy gap of 2.53 eV, which makes these layers a reliable material for photocatalytic application. The photocatalytic activity of Sb_2S_3 for degrading methylene blue under visible light was investigated. The degradation rate of the amorphous Sb_2S_3 layer toward methylene blue is highly efficient. This is due to the broad-spectrum response and the proper valence band position of Sb_2S_3. This investigation indicates that Sb_2S_3 is an excellent visible-light responsive photocatalyst for degrading organic pollutants.

Author contributions

Mohammed M. Gomaa: conceptualization, data curation, formal analysis, investigation, methodology, writing – original draft. Mohamed H. Sayed: conceptualization, data curation, formal analysis, investigation, methodology, writing – original draft. Mahmoud S. Abdel-Wahed: conceptualization, methodology, data curation, formal analysis, investigation, writing – original draft. Mostafa Boshta: funding acquisition, project administration, resources, supervision, validation, writing – original draft.

Conflicts of interest

The authors declare no competing interests.

Acknowledgements

The authors acknowledge the financial support from the National Research Centre Fund, through in-house project numbers 13020240 and 13040124.

Notes and references

1 Y. Zhang, P. Li, Y. Li, M. Wang, L. Fan and Z. Zheng, Synthesis of Sb_2S_3 films on conducting substrate and its application in hybrid solar cell devices, *Funct. Mater. Lett.*, 2015, **8**, 17–20.

2 J. Li, P. Jiménez-Calvo, E. Paineau and M. N. Ghazzal, Metal chalcogenides based heterojunctions and novel nanostructures for photocatalytic hydrogen evolution, *Catalysts*, 2020, **10**, 89.

3 Y. Liang, Y. Yang, K. Xu, T. Yu, S. Yao, Q. Peng and C. Yuan, Crystal plane dependent electrocatalytic performance of NiS_2 nanocrystals for hydrogen evolution reaction, *J. Catal.*, 2020, **381**, 63–69.

4 M. Dai and R. Wang, Synthesis and applications of nanostructured hollow transition metal chalcogenides, *Small*, 2021, **17**, 1–28.
5 B. T. Gadisa, R. Appiah-Ntiamoah and H. Kim, Amorphous iron sulfide nanowires as an efficient adsorbent for toxic dye effluents remediation, *Environ. Sci. Pollut. Res.*, 2019, **26**, 2734–2746.
6 C. H. Lai, M. Y. Lu and L. J. Chen, Metal sulfide nanostructures: synthesis, properties and applications in energy conversion and storage, *J. Mater. Chem.*, 2012, **22**, 19–30.
7 J. Cheng, Y. Pan, J. Zhu, Z. Li, J. Pan and Z. Ma, Hybrid network CuS monolith cathode materials synthesized via facile in situ melt-diffusion for Li-ion batteries, *J. Power Sources*, 2014, **257**, 192–197.
8 S. L. Lee and C. Chang, Recent Progress on Metal Sulfide Composite Hydrogen Production, *Catalysts*, 2019, **9**, 1–25.
9 N. Jiang, Q. Tang, M. Sheng, B. You, D. E. Jiang and Y. Sun, Nickel sulfides for electrocatalytic hydrogen evolution under alkaline conditions: a case study of crystalline NiS, NiS_2, and Ni_3S_2 nanoparticles, *Catal. Sci. Technol.*, 2016, **6**, 1077–1084.
10 S. Sharma and N. Khare, Sensitization of narrow band gap Bi_2S_3 hierarchical nanostructures with polyaniline for its enhanced visible-light photocatalytic performance, *Colloid Polym. Sci.*, 2018, **296**, 1479–1489.
11 M. M. Gomaa, G. RezaYazdi, M. Rodner, G. Greczynski, M. Boshta, M. B. S. Osman, V. Khranovskyy, J. Eriksson and R. Yakimova, Exploring NiO nanosize structures for ammonia sensing, *J. Mater. Sci.: Mater. Electron.*, 2018, **29**, 11870–11877.
12 M. Luo, Y. Liu, J. Hu, J. Li, J. Liu and R. M. Richards, General strategy for one-pot synthesis of metal sulfide hollow spheres with enhanced photocatalytic activity, *Appl. Catal., B*, 2012, **125**, 180–188.
13 M. M. Gomaa, M. H. Sayed and M. Boshta, Engineering of NiO/ZnO core–shell nanostructure via facile chemical processes for environmental application, *ECS J. Solid State Sci. Technol.*, 2023, **12**, 023002.
14 H. Hao and X. Lang, Metal Sulfide Photocatalysis: Visible-Light-Induced Organic Transformations, *ChemCatChem*, 2019, **11**, 1378–1393.
15 Z. Mamiyev and N. O. Balayeva, Metal Sulfide Photocatalysts for Hydrogen Generation: A Review of Recent Advances, *Catalysts*, 2022, **12**, 1316.
16 Q. Gong, T. Gao, T. Hu and G. Zhou, Synthesis and electrochemical energy storage applications of micro/nanostructured spherical materials, *Nanomaterials*, 2019, **9**, 1207.
17 G. M. Tomboc, B. T. Gadisa, J. Joo, H. Kim and K. Lee, Hollow structured metal sulfides for Photocatalytic hydrogen generation, *ChemNanoMat*, 2020, **6**, 850–869.
18 J. K. Kim, S. K. Park, J. S. Park and Y. C. Kang, Uniquely structured composite microspheres of metal sulfides and carbon with cubic nanorooms for highly efficient anode materials for sodium-ion batteries, *J. Mater. Chem. A*, 2019, **7**, 2636–2645.
19 X. Fang, T. Zhai, U. K. Gautam, L. Li, L. Wu, Y. Bando and D. Golberg, ZnS nanostructures: from synthesis to applications, *Prog. Mater. Sci.*, 2011, **56**, 175–287.
20 X. Chen, J. Zhang, J. Zeng, Y. Shi, S. Lin, G. Huang, H. Wang, Z. Kong, J. Xi and Z. Ji, MnS coupled with ultrathin MoS_2 nanolayers as heterojunction photocatalyst for high photocatalytic and photoelectrochemical activities, *J. Alloys Compd.*, 2019, **771**, 364–372.
21 P. Kumari, P. Chandran and S. S. Khan, Synthesis and characterization of silver sulfide nanoparticles for photocatalytic and antimicrobial applications, *J. Photochem. Photobiol., B*, 2014, **141**, 235–240.
22 D. Heift, Iron Sulfide Materials: Catalysts for Electrochemical Hydrogen Evolution, *Inorganics*, 2019, **7**, 75.
23 G. Ma, H. Peng, J. Mu, H. Huang, X. Zhou and Z. Lei, In situ intercalative polymerization of pyrrole in graphene analogue of MoS_2 as advanced electrode material in supercapacitor, *J. Power Sources*, 2013, **229**, 72–78.
24 M. M. Gomaa, M. H. Sayed, M. S. Abdel-Wahed and M. Boshta, A facile chemical synthesis of nanoflake NiS_2 layers and their photocatalytic activity, *RSC Adv.*, 2022, **12**, 10401–10408.
25 J. Rakspun, N. Kantip, V. Vailikhit, S. Choopun and A. Tubtimtae, Multi-phase structures of boron-doped copper tin sulfide nanoparticles synthesized by chemical bath deposition for optoelectronic devices, *J. Phys. Chem. Solids*, 2018, **115**, 103–112.
26 E. M. Mkawi, R. Almalki and Y. Al-Hadeethi, Influence of different concentrations of $SbCl_3$ salt on the properties of Sb_2S_3 nanobars prepared by the solvothermal method for solar cell application, *Opt. Mater. Express*, 2021, **11**, 2219.
27 J. H. Chen, S. K. Chiu, J. De Luo, S. Y. Huang, H. A. Ting, M. Hofmann, Y. P. Hsieh and C. C. Ting, Robust formation of amorphous Sb_2S_3 on functionalized graphene for high-performance optoelectronic devices in the cyan-gap, *Sci. Rep.*, 2020, **10**, 1–8.
28 A. Molla, M. Sahu and S. Hussain, Synthesis of tunable band gap semiconductor nickel sulphide nanoparticles: rapid and round the clock degradation of organic dyes, *Sci. Rep.*, 2016, **6**, 1–11.
29 M. Sun, D. Li, W. Li, Y. Chen, Z. Chen, Y. He and X. Fu, New photocatalyst, Sb_2S_3, for degradation of methyl orange under visible-light irradiation, *J. Phys. Chem. C*, 2008, **112**, 18076–18081.
30 F. Li, L. Zhang, C. Hu, X. Xing, B. Yan, Y. Gao and L. Zhou, Enhanced azo dye decolorization through charge transmission by Σ-Sb^{3+}-azo complexes on amorphous Sb_2S_3 under visible light irradiation, *Appl. Catal., B*, 2019, **240**, 132–140.
31 J. Tang, J. Li, Y. Cheng, P. Huang and Q. Deng, Facile hydrothermal-carbonization preparation of carbon-modified Sb_2S_3 composites for photocatalytic degradation of methyl orange dyes, *Vacuum*, 2015, **120**, 96–100.
32 K. H. Park, J. Choi, H. J. Kim, J. B. Lee and S. U. Son, Synthesis of antimony sulfide nanotubes with ultrathin walls via gradual aspect ratio control of nanoribbons, *Chem. Mater.*, 2007, **19**, 3861–3863.

33 V. A. V. Schmachtenberg, G. Tontini, J. A. Koch, G. D. L. Semione and V. Drago, Low temperature solventless syntheses of nanocrystalline nickel sulfides with different sulfur sources, *J. Phys. Chem. Solids*, 2015, **87**, 253–258.

34 A. Radoń, S. Łoński, T. Warski, R. Babilas, T. Tański, M. Dudziak and D. Łukowiec, Catalytic activity of non-spherical shaped magnetite nanoparticles in degradation of Sudan I, Rhodamine B and Methylene Blue dyes, *Appl. Surf. Sci.*, 2019, **487**, 1018–1025.

35 G. Zhu, X. Huang, M. Hojamberdiev, P. Liu, Y. Liu, G. Tan and J. P. Zhou, Preparation of Sb_2S_3 film on functional organic self-assembled monolayers by chemical bath deposition, *J. Mater. Sci.*, 2011, **46**, 700–706.

36 H. Maghraoui-Meherzi, T. Ben Nasr, N. Kamoun and M. Dachraoui, Structural, morphology and optical properties of chemically deposited Sb_2S_3 thin films, *Phys. Rev. B: Condens. Matter Mater. Phys.*, 2010, **405**, 3101–3105.

37 N. S. Tezel, F. M. Tezel and I. A. Kariper, Surface and electro-optical properties of amorphous Sb_2S_3 thin films, *Appl. Phys. A: Mater. Sci. Process.*, 2019, **125**, 1–16.

38 M. Calixto-Rodriguez, H. Martínez, Y. Peña, O. Flores, H. E. Esparza-Ponce, A. Sanchez-Juarez, J. Campos-Alvarez and P. Reyes, A comparative study of the physical properties of Sb_2S_3 thin films treated with N_2 AC plasma and thermal annealing in N_2, *Appl. Surf. Sci.*, 2010, **256**, 2428–2433.

39 S. A. Zaki, M. I. Abd-Elrahman and A. A. Abu-Sehly, Optical and electrical properties of amorphous Sb_2S_3 thin films: effect of the film thickness, *J. Non-Cryst. Solids*, 2021, **552**, 120318.

40 Y. Gutiérrez, A. P. Ovvyan, G. Santos, D. Juan, S. A. Rosales, J. Junquera, P. García-Fernández, S. Dicorato, M. M. Giangregorio, E. Dilonardo, F. Palumbo, M. Modreanu, J. Resl, O. Ishchenko, G. Garry, T. Jonuzi, M. Georghe, C. Cobianu, K. Hingerl, C. Cobet, F. Moreno, W. H. P. Pernice and M. Losurdo, Interlaboratory study on Sb_2S_3 interplay between structure, dielectric function, and amorphous-to-crystalline phase change for photonics, *iScience*, 2022, **25**, 104377.

41 J. S. Eensalu, A. Katerski, E. Kärber, I. O. Acik, A. Mere and M. Krunks, Uniform Sb_2S_3 optical coatings by chemical spray method, *Beilstein J. Nanotechnol.*, 2019, **10**, 198–210.

42 V. Vinayakumar, C. R. O. Hernández, S. Shaji, D. A. Avellaneda, J. A. A. Martinez and B. Krishnan, Effects of rapid thermal processing on chemically deposited antimony sulfide thin films, *Mater. Sci. Semicond. Process.*, 2018, **80**, 9–17.

43 A. Kuruvilla, M. Francis, K. S. Sudheer and M. Lakshmi, Replacement of sulphur with selenium in antimony sulphide thin films, *Bull. Mater. Sci.*, 2022, **45**, 66.

44 D. Zhang, B. Chen, S. Wang, Y. Shen, C. Wang, Z. Wang, L. Wang and Y. Cheng, Boosting reversibility of conversion/alloying reactions for sulfur-rich antimony-based sulfides with extraordinary potassium storage performance, *ACS Mater. Lett.*, 2022, **4**, 2604–2612.

45 P. A. Nwofe and M. Sugiyama, Influence of deposition time and annealing treatments on the properties of chemically deposited $Sn_2Sb_2S_5$ thin films and photovoltaic behavior of $Sn_2Sb_2S_5$-based solar cells, *Z. Naturforsch. A*, 2020, **75**, 887–901.

46 K. H. Park, J. Choi, J. Chun, H. J. Kim and S. U. Son, Low-temperature synthesis of ultrathin Sb_2S_5 nanofibers and their application as highly selective Pb-adsorbents in water, *Chem. Commun.*, 2008, **14**, 1659–1661.

47 W. E. Morgan, W. J. Stec and J. R. Van Wazer, Inner-orbital binding-energy shifts of antimony and bismuth compounds, *Inorg. Chem.*, 1973, **12**, 953–955.

48 S. Shaji, L. V. Garcia, S. L. Loredo, B. Krishnan, J. A. Aguilar Martinez, T. K. Das Roy and D. A. Avellaneda, Antimony sulfide thin films prepared by laser assisted chemical bath deposition, *Appl. Surf. Sci.*, 2017, **393**, 369–376.

49 W. Xiang, Q. Tian, C. Zhong, Y. Deng, X. Han and W. Hu, A Solution-based method for synthesizing pyrite-type ferrous metal sulfide microspheres with efficient OER activity, *Chem.–Asian J.*, 2020, **15**, 2231–2238.

50 A. Baral, A. Dhara, A. Sinha and N. Mukherjee, Chemically synthesized Sb_2S_3 hollow-spheres for significantly fast and reliable visible light driven dye photodegradation, *Spectrochim. Acta, Part A*, 2021, **250**, 119368.

51 M. M. Gomaa, G. R. Yazdi, S. Schmidt, M. Boshta, V. Khranovskyy, F. Eriksson, B. S. Farag, M. B. S. Osman and R. Yakimova, Effect of precursor solutions on the structural and optical properties of sprayed NiO thin films, *Mater. Sci. Semicond. Process.*, 2017, **64**, 32–38.

52 I. Grozdanov, M. Ristov, G. Sinadinovski and M. Mitreski, Fabrication of amorphous Sb_2S_3 films by chemical deposition, *J. Non-Cryst. Solids*, 1994, **175**, 77–83.